

DFG–Schwerpunktprogramm 1114

Mathematical methods for time series analysis and digital image processing

Instantaneous polarization attributes in the time-frequency domain and wave field separation

M. S. Diallo

M. Kulesh

M. Holschneider

F. Scherbaum

Preprint 57

Preprint Series DFG-SPP 1114

Preprint 57

October 2004

The consecutive numbering of the publications is determined by their chronological order.

The aim of this preprint series is to make new research rapidly available for scientific discussion. Therefore, the responsibility for the contents is solely due to the authors. The publications will be distributed by the authors.

ISBN 3-88722-625-9

Instantaneous polarization attributes in the time-frequency domain and wave field separation

M. S. Diallo¹, M. Kulesh¹, M. Holschneider¹, F. Scherbaum²

¹ *Institute for Mathematics, University of Potsdam, Am neuen Palais 10, 14469 Potsdam Germany*

² *Institute for Geoscience, University of Potsdam, Karl-Liebknecht-Strasse 24-25, 14414 Potsdam, Germany*

Contact author's email: mamadou@math.uni-potsdam.de

SUMMARY

We introduce a method of wave field separation from multicomponent data sets based on the use of the continuous wavelet transform. Our method is a further generalization of the approach proposed by (Morozov & Smithson, 1996) in that by using the continuous wavelet transform, we can achieve a better separation of wave types by designing the filter in the time-frequency domain. Furthermore, using the instantaneous polarization attributes defined in the wavelet domain, we show how to construct filters tailored to separate different wave types (elliptically or linearly polarized) followed by an inverse wavelet transform to obtain the desired wave type in the time domain. Using synthetic and experimental data, we show how the present method can be used for wave field separation.

Key words: wavelet transform, polarization attributes, multicomponent signal

1 INTRODUCTION

Multicomponent seismic records entail important information about the subsurface that are very often overlooked because of the lack of appropriate tool for their extraction and interpretation. (Vidale, 1986; Rene et al., 1986; Li & Crampin, 1991) defined instantaneous

polarization attributes for the characterization of Rayleigh waves and the observation of shear-wave splitting. Both methods were applied to 2-component data and cannot be easily extended to higher component data (Morozov & Smithson, 1996). The latter authors proposed a method based on variational principle that allows a generalization to any number of components where they briefly addressed the potential of using the instantaneous polarization attributes for wave field separation and shear wave splitting identification. (Park, 1987) proposed techniques that provide the polarization estimates in the frequency domain. The common characteristics of the methods mentioned above is that they all operate exclusively either in the time domain or frequency domain. However when several wave type arrivals are observed around the same time in a record, it becomes difficult to characterize the polarization attributes of either arrivals by using methods that operate exclusively in the time domain or in the frequency domain. To circumvent this problem, the development of techniques that simultaneously handle the time and frequency dependence of the polarization attributes is needed. In (Reading et al., 2001) a polarization filter was designed following (Samson & Olson, 1981). The method consisted of applying the Fourier transform on successive segments of the 3C input data. Afterwards the frequency dependent eigenvalues (eigenvectors) are computed from 3x3 spectral matrix in each segment and used for the construction of the polarization filter designed only in the frequency domain. A more natural way of bringing the time- frequency capability into polarization analysis would be to use the continuous wavelet transform. Such an approach has been recently proposed by (Diallo et al., 2004) which overcomes some of the difficulties mentioned above but was limited to 2-component record. Here we present an extension of (Morozov & Smithson, 1996) to the time-frequency domain to improve the potential of using the instantaneous attribute for filtering and wave field separation, shear wave splitting investigation for any number of component.

2 INSTANTANEOUS POLARIZATION ATTRIBUTES

2.1 Time domain

Let $\mathbf{S}(t) = (S_x(t), S_y(t), S_z(t))$ be a seismic vector made of the three component seismic signal recorded from 3 orthogonal direction x , y and z respectively. Let $\mathbf{S}^c = (S_x^c(t), S_y^c(t), S_z^c(t))$ be the analytic multicomponent signal obtained from the use of Hilbert transform by zeroing the negative frequency part of the signal and doubling the positive frequency part:

$$\mathbf{S}^c(t) = \mathbf{S}(t) + i \mathbf{S}^H(t)$$

where $(.)^H$ indicates the Hilbert transform. The element of the analytic multicomponent signal are given explicitly as

$$S_k^c(t) = S_k(t) + i S_k^H(t), \quad k = x, y, z.$$

(Morozov & Smithson, 1996) show that the determination of the polarization attributes $\mathbf{S}(t)$ can be achieved by finding the phase factor $\phi(t)$ in the expression below

$$\mathbf{S}^c(t) = \mathbf{A}(t)e^{i\phi(t)},$$

where $\phi(t)$ is the unique real-valued phase of the multicomponent signal responsible for the fast time variation and $\mathbf{A}(t)$, the slow time varying complex-valued vector function that contains the polarization, the amplitude and time phase shift information of the multicomponent signal. The phase function is determined through a variational approach that maximize the following functional

$$\Phi(e^{-i\phi}\mathbf{S}^c(t)) = \sum_k \Re(e^{-i\phi}S_k^c(t))^2 + \varepsilon \left(\sum_k \Re(e^{-i\phi}S_k^c(t)) \right)^2,$$

where $\Re(\cdot)$ implies that the real part of argument is considered and $\varepsilon \ll 1$ is a regularization parameter to stabilize the calculation when the first term becomes constant.

The phase function $\phi(t) = \phi_0(t)$ that maximizes the above functional is given by (Morozov & Smithson, 1996)

$$\phi_0(t) = \frac{1}{2} \arg [B(t) + \varepsilon C(t)] + \pi n, \quad n \in \mathbb{N},$$

where

$$B(t) = \frac{1}{2} \sum_k S_k^c(t)^2 \text{ and } C(t) = \frac{1}{2} \left(\sum_k S_k^c(t) \right)^2.$$

Given the phase factor $\phi_0(t)$, the instantaneous vectors for the semi-major axis $\mathbf{R}(t)$, the semi-minor axis $\mathbf{r}(t)$ of an ellipse lying in a plane in the 3-D space and the amplitude of the multicomponent signal $\mathbf{A}(t)$ are derived:

$$\mathbf{R}(t) = \Re[e^{-i\phi_0(t)} \mathbf{S}^c(t)],$$

$$\mathbf{r}(t) = \Re[e^{-i(\phi_0(t)+\pi/2)} \mathbf{S}^c(t)],$$

$$\mathbf{A}(t) = \sqrt{\Phi(e^{-i\phi_0(t)} \mathbf{S}^c(t))}.$$

Other parameters such as the ellipticity ratio, the dip angle, the strike angle and phase difference can then be easily calculated from the semi-minor and semi-major axis $\mathbf{r}(t)$ and $\mathbf{R}(t)$ respectively. Note that since the phase $\phi_0(t)$ is determined with an uncertainty modulo $n\pi$, the orientation of the axes is unknown.

2.2 Time-frequency domain

The wavelet transform of a signal $S(t) \in L^2(\mathbb{R})$ with respect to a mother wavelet $g(t)$ is defined as follows,

$$\mathcal{W}_g S(b, a) = \int_{-\infty}^{+\infty} \frac{1}{a} g^* \left(\frac{t-b}{a} \right) S(t) dt = \langle g_{b,a}, S \rangle, \quad (1)$$

where $\langle \cdot, \cdot \rangle$ is the L^2 -scalar product and $g_{b,a}(t) = \frac{1}{a} g((t-b)/a)$ is generated from g through dilation ($a > 0$) and translation ($b \in \mathbb{R}$). The symbol $*$ denotes the usual complex conjugate. Applying equation (1) on $\mathbf{S}(t)$ component wise yields $\mathcal{W}_g \mathbf{S}(b, a)$ which consist of the respective wavelet transforms $\mathcal{W}_g S_k(b, a)$ of $S_k(t)$. The wavelet g is assumed to be a function well localized in the time and frequency domains and obeying the oscillation condition

$$\int_{-\infty}^{+\infty} g(t) dt = 0.$$

The wavelet transform can be expressed in terms of the Fourier transform $\hat{\mathbf{S}}$ of \mathbf{S} ,

$$\mathcal{W}_g \mathbf{S}(b, a) = \int_{-\infty}^{+\infty} \hat{g}^*(a\zeta) e^{2\pi i b \zeta} \hat{\mathbf{S}}(\zeta) d\zeta,$$

From this we see that the inverse $1/a$ of the scale may be associated with a frequency

measured in units of the central frequency of g . If the central frequency of the wavelet is assumed to be f_0 , then each scale a can be related to the physical frequency f by $a = f_0/f$. Therefore, if we select a wavelet with a unit central frequency, we can directly obtain the physical frequency by taking the inverse of the scale. For the sake of clarity, we will consider a wavelet with unit central frequency and proceed with the physical frequency instead of the scale in the next sections. The multicomponent signal $\mathbf{S}(t)$ can be recovered from its wavelet transform (again component wise !) as follows,

$$\mathbf{S}(t) = \frac{1}{C_g} \int_0^\infty \int_{-\infty}^{+\infty} \frac{1}{a} g\left(\frac{t-b}{a}\right) \mathcal{W}_g \mathbf{S}(b, a) \frac{db da}{a},$$

where the constant C_g is defined below.

In this paper we limit ourselves to real-valued signals and admissible, progressive analyzing wavelets, i.e., we assume $\hat{g}(f) = 0$ for $f \leq 0$, and that the constant $C_g = \int_0^\infty |\hat{g}(f)|^2 \frac{df}{f}$ is finite. With this restriction, the wavelet transform of the multicomponent signal $\mathbf{S}(\mathbf{t})$ is equivalent to the wavelet transform of the multicomponent analytical signal $\mathbf{S}^c(t)$ (Holschneider, 1995).

Following the approach outlined in the previous section, it is possible to redefine all the instantaneous attributes in the time-frequency in terms of $\mathcal{W}_g \mathbf{S}(b, a)$ and $\phi_0(b, a)$. The resulting semi-major, semi-minor and the instantaneous amplitude are

$$\begin{aligned} \mathbf{R}(b, a) &= \Re[e^{-i\phi_0(b,a)} \mathcal{W}_g \mathbf{S}(b, a)], \\ \mathbf{r}(b, a) &= \Re[e^{-i(\phi_0(b,a)+\pi/2)} \mathcal{W}_g \mathbf{S}(b, a)], \\ \mathbf{A}(b, a) &= \sqrt{\Phi(e^{-i\phi_0(b,a)}) \mathcal{W}_g \mathbf{S}(b, a)}, \end{aligned} \tag{2}$$

respectively. The ellipticity ratio $\rho(b, a)$ is then derived as

$$\rho(b, a) = \frac{\|\mathbf{r}(b, a)\|}{\|\mathbf{R}(b, a)\|}.$$

From equation (2) we have

$$\Re \mathcal{W}_g \mathbf{S}(b, a) = \mathbf{R}(b, a) \cos(\phi_0(b, a)) - \mathbf{r}(b, a) \sin(\phi_0(b, a)), \tag{3}$$

$$\Im \mathcal{W}_g \mathbf{S}(b, a) = \mathbf{R}(b, a) \sin(\phi_0(b, a)) + \mathbf{r}(b, a) \cos(\phi_0(b, a)). \tag{4}$$

By using equations (3) and (4) we can express the full wavelet transform $\mathcal{W}_g \mathbf{S}(b, a)$ of the

multicomponent signal in terms of the ellipticity parameters $\mathbf{R}(b, a)$, $\mathbf{r}(b, a)$ and the phase factors $\phi_0(b, a)$ as:

$$\mathcal{W}_g \mathbf{S}(b, a) = \Re \mathcal{W}_g \mathbf{S}(b, a) + i \Im \mathcal{W}_g \mathbf{S}(b, a). \quad (5)$$

The ellipse in the 3-D space is determined by the major axis which is well defined expect for a circular particle motion in which case the presence of noise will introduce an artificial major axis. To avoid such problem, (Schimmel & Gallart, 2003) use the planarity vector

$$\mathbf{p}(b, a) = \mathbf{R}(b, a) \times \mathbf{r}(b, a) = (p_x(b, a), p_y(b, a), p_z(b, a))$$

for circular or elliptical motion and should stay in the same direction if the ellipse remains in the same plane. To track the position of the ellipse in the 3-D space, we determine the different angles between \mathbf{p} and the orthogonal axes x , y and z at each point (b, a) . We denote these angles $\theta_x(b, a)$, $\theta_y(b, a)$ and $\theta_z(b, a)$ respectively, where

$$\theta_k(b, a) = \cos^{-1} \left[\frac{|p_k(b, a)|}{\|\mathbf{p}(b, a)\|} \right] \quad k = x, y, z, \quad \theta_k(b, a) \in \left[0, \frac{\pi}{2} \right]. \quad (6)$$

Using $\mathbf{R}(b, a)$, $\mathbf{r}(b, a)$ and $\mathbf{p}(b, a)$ and other derived instantaneous polarization parameters it is possible to design filters that enable one to select or analyze wave types with specific polarization attributes. Application may include surface filtering/analysis, shear wave splitting investigation, separation of converted waves, removal of out-plane energy, etc. For an efficient filter construction, earlier techniques that were mostly designed either in the time (Kanasewich, 1981; Perelberg & Hornbostel, 1994; Morozov & Smithson, 1996; Shieh, 1997) or frequency domain (Park, 1987) can be revisited in the light of the present contribution.

3 APPLICATION TO FILTERING

3.1 Synthetic example

In the following we show how to use the instantaneous attributes defined in wavelet domain for the purpose of separating different wave types. We simulate a 3 component record with seismic events consisting of a superposition of elliptically and linearly polarized events. The simulation is not based on an actual physical model but rather thought as a simplified

illustration of the filtering principle. The actual simulated 3 component record is depicted in Figure (1). It consists of an elliptically polarized events in the $(x - y)$ plane from 1s to 5s, a second elliptically polarized events in the $(x - z)$ plane from 5s to 9s, a third elliptically polarized event in the $(y - z)$ plane from 9s to 15s and finally a mixture of linearly and elliptically polarized events having different frequency content between 15s and 20s. To extract an elliptically polarized event in any plane we design a filter constrained by the range of reciprocal ellipticity and the direction of $\mathbf{p}(b, a)$ as given by the equation (6).

To isolate the elliptically polarized event on the $(x - y)$ plane, one would first identify the region in the time-frequency plane where $\theta_z(b, a) = 0$ (between 1 and 5s in time in Figure (2d) and corresponding to the ellipticity ratio in the same time window in Figure (2a) and where the reciprocal ellipticity ratio $\rho(b, a)$ is with a certain range (i.e $\rho(b, a) \approx 0.6$ in the present example as shown in Figure (2a)). Note that the linear event is not observed here because its ellipticity ratio is zero and corresponds to the background color for this plot.

Next one sets the values of $\mathbf{R}(b, a)$, $\mathbf{r}(b, a)$ and $\phi_0(b, a)$ that fall outside the region delimited by the two previous concurrent constraints to zero and plug the resulting parameters $\mathbf{R}'(b, a)$, $\mathbf{r}'(b, a)$ and $\phi'_0(b, a)$ into equations (4) and (3). Finally taking the inverse-wavelet transform of equation (5) yields the multicomponent signal that emphasizes the desired event. The procedure outlined above can be adapted to extract the elliptically polarized events in the $(x - y)$ and $(y - z)$ planes. In Figure (1a) we have chosen to detect the events on the $(x - z)$ plane where from the initial synthetic we have one distinguishable elliptical event than extend from nearly 5s to 10s but also the elliptical event in the time window between 15 and 20s which is superimposed the linear one. The dashed curves in Figure (1a) depict the filtering results which replicate pretty well the initial synthetic as desired.

3.2 Experimental data

The real seismogram used in this study is a 3 component record from an explosive-source experiment aimed at imaging the Dead Sea Transform in the middle-east (Group, 2000). The horizontal seismograms were rotated into radial and transversal components using the

shot/receiver azimuth obtained from the survey geometry. Figure (3a) show the rotated seismograms. The methodology described in the previous section was applied to this seismograms to produce the polarization attributes in the time-frequency domain. The modulus of the wavelet transforms of each individual component of the record is shown in Figure (4) where depicting the location of some events in the time-frequency plane and the relative importance of their energy content codified into the color scale that grow from white for low amplitude to black for high amplitude arrival.

In Figure (5), polarization attribute that were used for an illustrative filtering approach are displayed. Figure (5a) corresponds to the reciprocal ellipticity which is normally close to one for either elliptically or circularly polarized events and to zero for linearly polarized event. A window of persistent elliptical polarization can be observed between approximately 3s and 5s in time, culminating around 5 Hz in the frequency axis. With the help of the direction of the planarity vector indicated by the different angles $\theta_k(b, a), k = x, y, z$ in Figures (5a), (5d) and (5c) respectively we can determine at each point (b, a) the direction of the energy arrival.

From Figure (5b) two regions where $\theta_x(b, a)$ is relatively small can be observed in the earlier arrival times. The first region is contained in a narrow frequency strip that extend from 2s to nearly 4s and would correspond to the lower frequency region with events of low elliptical polarization as can be seen in the corresponding time-frequency window in Figure (5a). The second region covers a wider frequency range that goes from 4 to 10 Hz and is limited to the time window between 2.5 s to 4s. The arrivals in this region are linearly polarized as indicated by the small value of $\rho(b, a)$ from Figure (5a) in that region. The weak $\theta_x(b, a)$ values in this region suggests that the direction of incoming energy is dominantly in the $(y - z)$ plane. By performing this analysis on multicomponent data one can easily identified the out-of-plane energy arrival and construct appropriate filter to reduce its contamination of the in-line and vertical components.

From Figure (5c) the region that would correspond to the energetic event with elliptical polarization mentioned earlier is dominant blue to light blue in color corresponding to small

angles $\theta_y(b, a)$ which means that the planarity vector is nearly parallel to the y -axis in that region. Such a behavior can be interpreted as an indication that the energy arrival in the time-frequency window under observation is mostly contained in the $(x - z)$ plane. The weak $\theta_y(b, a)$ values in this region suggests that the direction of incoming energy is dominantly in the $(x - z)$ plane. By performing this analysis on multicomponent data one can easily identified the out-of-plane energy arrival and construct appropriate filter to reduce its contamination of the in-line and vertical components.

Figure (3b) is an illustration of how the information form $\rho(b, a)$ and $\theta_k(b, a)$ can be used for wave type filtering. This figure show essentially seismic arrival with a polarization contained in the horizontal $(x - y)$ plane. It was obtained by selecting the region in the time-frequency plane where $\theta_z(b, a)$ is relatively small and then setting the corresponding $\mathbf{R}(b, a)$ and $\mathbf{r}(b, a)$ to zero followed by an inverse transform as was done with the synthetic example. With the result from only one seismogram it is difficult to speculate about the nature of the signal in such a the multicomponent seismogram. Because of the nature of source used in the experiment (explosive), shear wave arrivals would be relatively weak. The strong arrival observed on the filtered seismogram would probably correspond to P to S conversion or P-wave energy leaking into the horizontal component due to the offset. It's important to note that the energy arrival from the filtered vertical component is very weak which suggest that our filter is indeed capable of detecting the desired signal that is expected to be mainly in the x and y components.

Another important application of polarization analysis is the removal of out-of plane energy which is important in geologically complex areas. These out- of-plane energy arrivals may contaminate the inline signal which add to the difficulty of its analysis and may induce errors in the subsequent interpretation. Using the different components of the planarity vector $\theta_k(b, a)$, much of this energy can be attenuated. This is achieved by first normalizing the different $\theta_k(b, a)$ so that the range of each $\theta_k(b, a)$ is between 0 and 1. Afterwards, each normalized $\theta_k(b, a)$ is multiplied by the wavelet transform of the signal component along the the corresponding k -axis ($k = x, y, z$) followed by an inverse wavelet transform.

Figure (3c) is an illustration of the application of this approach to the multicomponent signal in Figure (3a) using the normalized $\theta_x(b, a)$, $\theta_y(b, a)$, $\theta_z(b, a)$ in Figures (5b-d) and the wavelet transforms of $S_x(t)$, $S_y(t)$, $S_z(t)$. One can see that the interference of wave-field in the time window from nearly 2.5s to 5s has been reduced making it much easier to identify the events in $S_x(t)$ and $S_z(t)$ that contribute to the Rayleigh arrival (large amplitude, low frequency events around 4s from both components). Also the event that might correspond to the Love wave is clearly singled out in $S_y(t)$ around 3.5s in time. We note that the most important effect of the filter for this particular example, in terms of amplitude reductions is observed along the $S_y(t)$ at around 4s. This would mean that around this time, some relatively considerable amount of out-of-plane energy arrival has been recorded along this component. This observation is in fact consistent with the interpretation of the $\theta_y(b, a)$ which has low values around this time window indicating that the arrivals are mostly from the x and z direction.

4 CONCLUSIONS

We have used the continuous wavelet transform to extend the polarization analysis technique for multicomponent data initially proposed by (Morozov & Smithson, 1996) into the time-frequency domain. We have discussed prospective ways for wave type separations based on the use the reciprocal ellipticity and the planarity vector. The introduction of the time-frequency capability into the polarization analysis method can improve the performance existing techniques used for wave types separation, surface wave analysis, directional filtering and shear wave splitting investigation.

ACKNOWLEDGMENTS

This project is supported by a grant from the Deutsche Forschungsgemeinschaft (DFG) within the framework of the priority program SPP 1114, "Mathematical methods for time series analysis and digital image processing". In subsection (3.2) we used data of the Controlled Source Array (CSA) experiment as part of the Dead Sea Research Project (DESERT,

<http://www.gfz-potsdam.de/pb2/pb22/projects/deadsea/ds-home.html>). DESERT was financed by the Deutsche Forschungsgemeinschaft (DFG), the GeoForschungsZentrum Potsdam (GFZ) and the Minerva Foundation. Instruments were provided by the Geophysical Instrument Pool Potsdam (GFZ) and the Free University of Berlin.

REFERENCES

- Diallo, M. S., Holschneider, M., Kulesh, M., Scherbaum, F., & Adler, F., 2004. Characterization of Seismic Waves Polarization Attributes Using Continuous Wavlet Transforms, *Submitted to Geophysics*.
- Group, D., 2000. Multinational geoscientific research kicks off in the Middle East, **81**(50), 609,616–617.
- Holschneider, M., 1995. *Wavelets: an analysis tool*, Clarendon Press, Oxford.
- Kanasewich, E. R., 1981. *Time series sequence analysis in geophysics*, University of Alberta Press, Edmonton, Alberta.
- Li, X. L. & Crampin, S., 1991. Complex component analysis of shear wave splitting: theory, *Geophys. J. Int.*, **107**, 597–604.
- Morozov, I. B. & Smithson, S. B., 1996. Instantaneous polarization attributes and directional filtering, *Geophysics*, **61**(2), 872–881.
- Park, J., 1987. Frequency dependent polarization analysis of high-frequency seismograms, *J. Geophys. Res.*, **92**, 12664–12674.
- Perelberg, A. I. & Hornbostel, S. C., 1994. Application of seismic polarization analysis, *Geophysics*, **59**, 119–130.
- Reading, A. M., Mao, W., & Gubbins, D., 2001. Polarization filtering for automatic picking of seismic data and improved converted phase detection, *Geophys. J. Int.*, **147**, 227–234.
- Rene, R. M., Fitter, J. L., Forsyth, P. M., Kim, K. Y., Murray, D. J., Walters, J. K., & Westerman, J. D., 1986. Multicomponent seismic studies using complex trace analysis, *Geophysics*, **51**, 1235–1251.
- Samson, J. C. & Olson, J. V., 1981. Data-adaptive polarization filter for multichannel geophysical data, *Geophysics*, **46**, 1423–1431.
- Schimmel, M. & Gallart, J., 2003. The use of instantaneous polarization attributes for seismic signal detection and image enhancement, *Geophys. J. Int.*, **155**, 653–668.
- Shieh, C. F., 1997. Estimation of shear-wave splitting using orthogonal transformation, *Geophysics*, **59**, 657–661.
- Vidale, J. E., 1986. Complex Polarization Analysis of Particle Motion, *BSSA*, **76**, 1393–1405.

5 LIST OF CAPTIONS

Figure 1. (a) Three synthetic signals simulating a 3 component record with elliptically polarized events contained in the (x-z), (x-y) and (y-z) planes. The late arrival on the three seismograms is a mixture of a linearly and elliptically polarized event with different frequency content. (b) Hodogram plot showing the the ellipses in the different polarization plane.

Figure 2. Instantaneous polarization attributes in the time-frequency domain: (a) the ellipticity ratio for the different events in the the multicomponent signal, (b) angle between the planarity vector and the x -axis, (c) angle between the planarity vector and the y -axis, (d) angle between the planarity vector and the z -axis. Note that for the first event $\theta_z(b, a) = 0$, for the second event, $\theta_y(b, a) = 0$, for the third event $\theta_x(b, a) = 0$. Only the linearly polarized event (high frequency) between 14s and 20s has non zero component for \mathbf{p} in all directions. For the elliptically polarized event in that time window, $\theta_y(b, a) = 0$.

Figure 3. Example of wave type separation. (a) Original data (inline, transversal and vertical). (b) Application of the polarization filter to to identify the seismic events polarized in he horizontal ($x - y$). The strong events here are most likely to be identified as converted waves. Note the low amplitudes on the filtered vertical component ($S_z^f(t)$) as expected. This residual energy is probably the result of leaking shear-wave energy on the vertical component. (c) Removal of the out-of-plane energy arrival. The application of such a filter (see text for explanation) has reduced the degree of interference between the different arrivals which in the identification of the different wave types.

Figure 4. Instantaneous polarization parameters used for the wave types separation. (a) The reciprocal ellipticity. (b) Angle between the direction of the planarity vector and the x -axis. (c) Angle between the direction of the planarity vector and the y -axis. (d) Angle between the direction of the planarity vector and the z -axis

Figure 5. Instantaneous polarization parameters used for the wave types separation. (a) The reciprocal ellipticity, (b) Angle between the direction of the planarity vector and the x -axis. (c) Angle between the direction of the planarity vector and the y -axis. (d) Angle between the direction of the planarity vector and the z -axis.

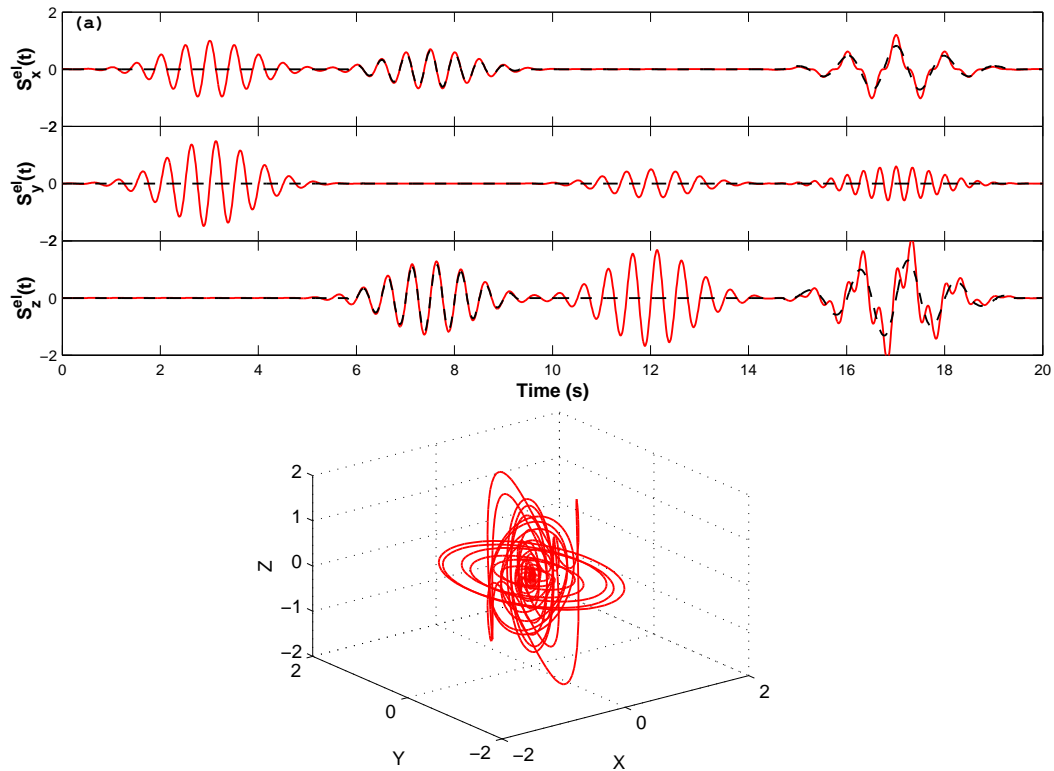


Figure 1. (a) Three synthetic signals simulating a 3 component record with elliptically polarized events contained in the (x-z), (x-y) and (y-z) planes. The late arrival on the three seismograms is a mixture of a linearly and elliptically polarized event with different frequency content. (b) Hodogram plot showing the the ellipses in the different polarization plane.

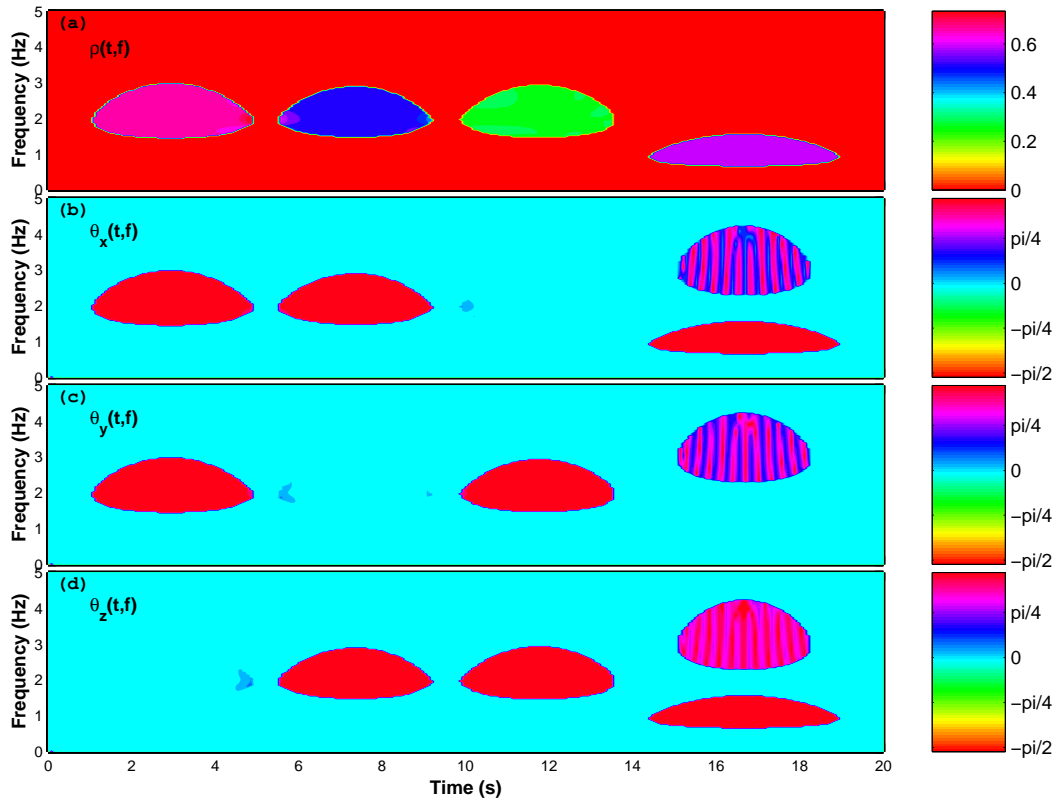


Figure 2. Instantaneous polarization attributes in the time-frequency domain: (a) the ellipticity ratio for the different events in the the multicomponent signal, (b) angle between the planarity vector and the x -axis, (c) angle between the planarity vector and the y -axis, (d) angle between the planarity vector and the z -axis. Note that for the first event $\theta_z(b, a) = 0$, for the second event, $\theta_y(b, a) = 0$, for the third event $\theta_x(b, a) = 0$. Only the linearly polarized event (high frequency) between 14s and 20s has non zero component for \mathbf{p} in all directions. For the elliptically polarized event in that time window, $\theta_y(b, a) = 0$.

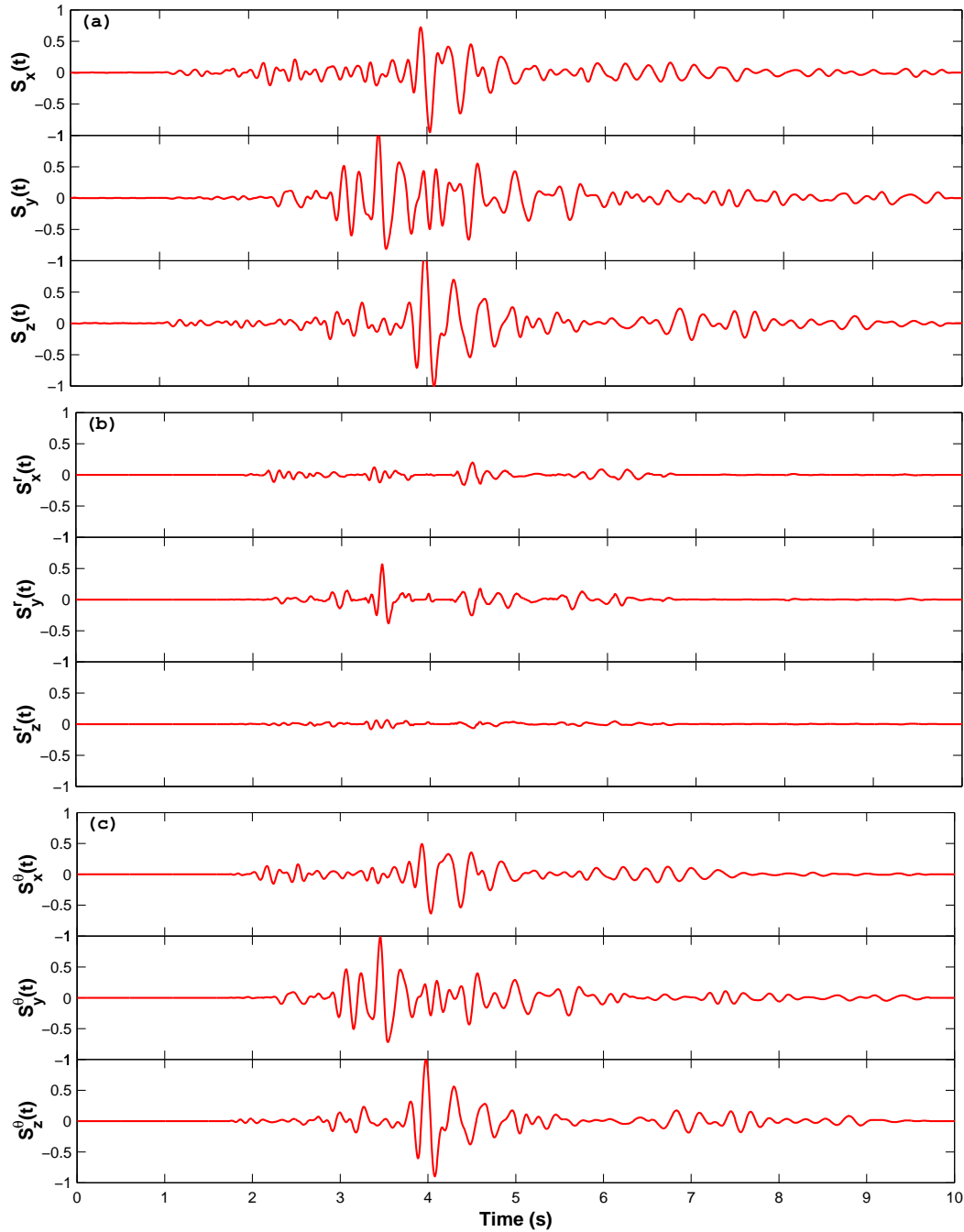


Figure 3. Example of wave type separation. (a) Original data (inline, transversal and vertical). (b) Application of the polarization filter to to identify the seismic events polarized in he horizontal ($x - y$). The strong events here are most likely to be identified as converted waves. Note the low amplitudes on the filtered

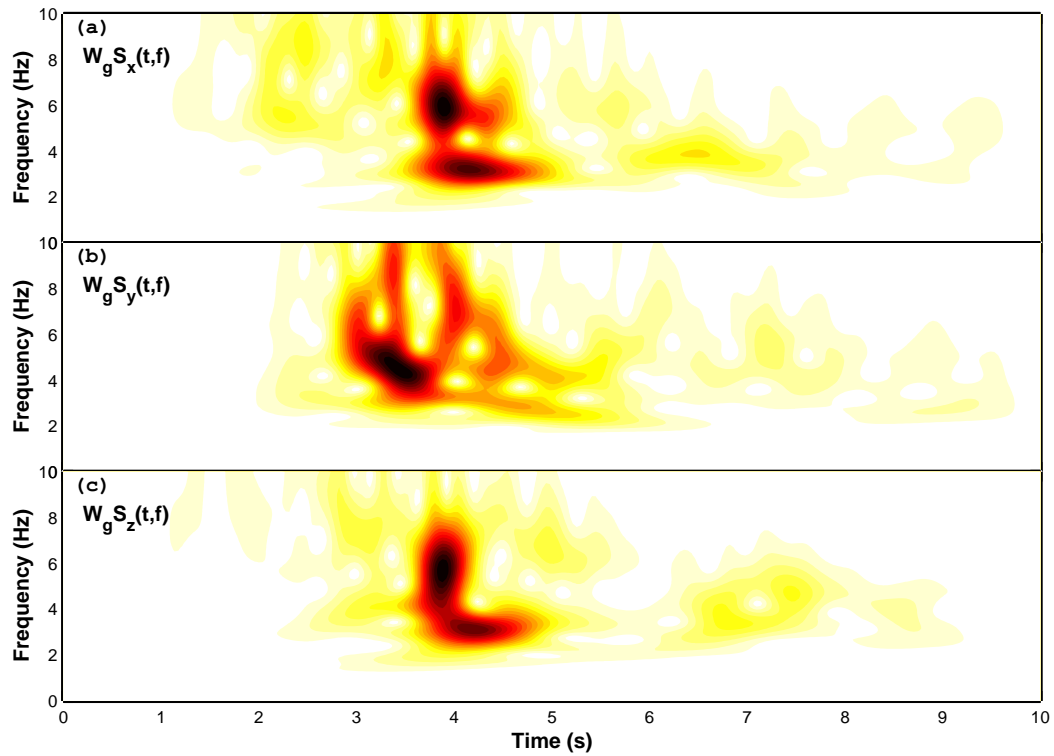


Figure 4. Instantaneous polarization parameters used for the wave types separation. (a) The reciprocal ellipticity. (b) Angle between the direction of the planarity vector and the x-axis. (c) Angle between the direction of the planarity vector and the y-axis. (d) Angle between the direction of the planarity vector and the z-axis

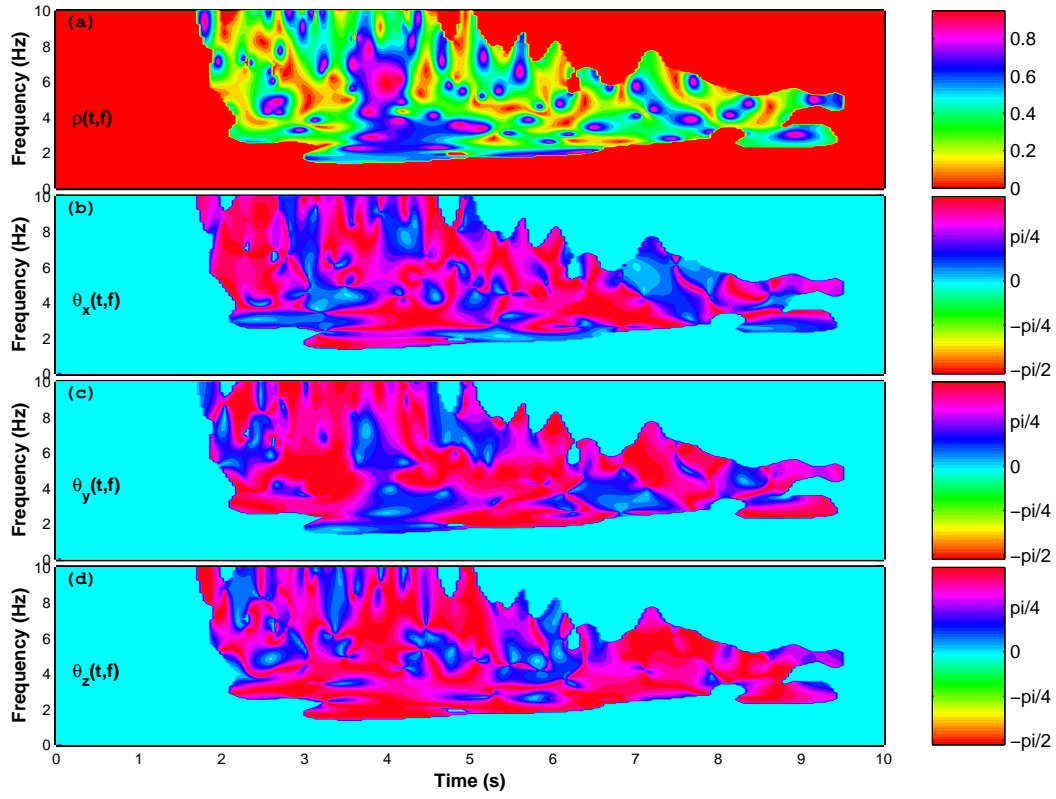


Figure 5. Instantaneous polarization parameters used for the wave types separation. (a) The reciprocal ellipticity, (b) Angle between the direction of the planarity vector and the x-axis. (c) Angle between the direction of the planarity vector and the y-axis. (d) Angle between the direction of the planarity vector and the z-axis.

Preprint Series DFG-SPP 1114

<http://www.math.uni-bremen.de/zetem/DFG-Schwerpunkt/SP.preprints.html>

Reports

- [1] W. Horbelt, J. Timmer, and H.U. Voss. Parameter estimation in nonlinear delayed feedback systems from noisy data. 2002 May. ISBN 3-88722-530-9.
- [2] A. Martin. Propagation of singularities. 2002 July. ISBN 3-88722-533-3.
- [3] T.G. Müller and J. Timmer. Fitting parameters in partial differential equations from partially observed noisy data. 2002 August. ISBN 3-88722-536-8.
- [4] G. Steidl, S. Dahlke, and G. Teschke. Coorbit spaces and banach frames on homogeneous spaces with applications to the sphere. 2002 August. ISBN 3-88722-537-6.
- [5] J. Timmer, T.G. Müller, I. Swameye, O. Sandra, and U. Klingmüller. Modeling the nonlinear dynamics of cellular signal transduction. 2002 September. ISBN 3-88722-539-2.
- [6] M. Thiel, M.C. Romano, U. Schwarz, J. Kurths, and J. Timmer. Surrogate based hypothesis test without surrogates. 2002 September. ISBN 3-88722-540-6.
- [7] K. Keller and H. Lauffer. Symbolic analysis of high-dimensional time series. 2002 September. ISBN 3-88722-538-4.
- [8] F. Friedrich, G. Winkler, O. Wittich, and V. Liebscher. Elementary rigorous introduction to exact sampling. 2002 October. ISBN 3-88722-541-4.
- [9] S.Albeverio and D.Belomestny. Reconstructing the intensity of non-stationary poisson. 2002 November. ISBN 3-88722-544-9.
- [10] O. Treiber, F. Wanninger, H. Führ, W. Panzer, G. Winkler, and D. Regulla. An adaptive algorithm for the detection of microcalcifications in simulated low-dose mammography. 2002 November. ISBN 3-88722-545-7.
- [11] M. Peifer, J. Timmer, and H.U. Voss. Nonparametric identification of nonlinear oscillating systems. 2002 November. ISBN 3-88722-546-5.
- [12] S.M. Prigarin and G. Winkler. Numerical solution of boundary value problems for stochastic differential equations on the basis of the gibbs sampler. 2002 November. ISBN 3-88722-549-X.
- [13] A. Martin, S.M.Prigarin, and G. Winkler. Exact numerical algorithms for linear stochastic wave equation and stochastic klein-gordon equation. 2002 November. ISBN 3-88722-547-3.
- [14] A. Groth. Estimation of periodicity in time series by ordinal analysis with application to speech. 2002 November. ISBN 3-88722-550-3.

- [15] H.U. Voss, J. Timmer, and J. Kurths. Nonlinear dynamical system identification from uncertain and indirect measurements. 2002 December. ISBN 3-88722-548-1.
- [16] U. Clarenz, M. Droske, and M. Rumpf. Towards fast non-rigid registration. 2002 December. ISBN 3-88722-551-1.
- [17] U. Clarenz, S. Henn, M. Rumpf, and K. Witsch. Relations between optimization and gradient flow with applications to image registration. 2002 December. ISBN 3-88722-552-X.
- [18] M. Droske and M. Rumpf. A variational approach to non-rigid morphological registration. 2002 December. ISBN 3-88722-553-8.
- [19] T. Preußner and M. Rumpf. Extracting motion velocities from 3d image sequences and spatio-temporal smoothing. 2002 December. ISBN 3-88722-555-4.
- [20] K. Mikula, T. Preußner, and M. Rumpf. Morphological image sequence processing. 2002 December. ISBN 3-88722-556-2.
- [21] V. Reitmann. Observation stability for controlled evolutionary variational inequalities. 2003 January. ISBN 3-88722-557-0.
- [22] K. Koch. A new family of interpolating scaling vectors. 2003 January. ISBN 3-88722-558-9.
- [23] A. Martin. Small ball asymptotics for the stochastic wave equation. 2003 January. ISBN 3-88722-559-7.
- [24] P. Maaß, T. Köhler, R. Costa, U. Parlitz, J. Kalden, U. Wichard, and C. Merkwirth. Mathematical methods for forecasting bank transaction data. 2003 January. ISBN 3-88722-569-4.
- [25] D. Belomestny and H. Siegel. Stochastic and self-similar nature of highway traffic data. 2003 February. ISBN 3-88722-568-6.
- [26] G. Steidl, J. Weickert, T. Brox, P. Mrázek, and M. Welk. On the equivalence of soft wavelet shrinkage, total variation diffusion, and sides. 2003 February. ISBN 3-88722-561-9.
- [27] J. Polzehl and V. Spokoiny. Local likelihood modeling by adaptive weights smoothing. 2003 February. ISBN 3-88722-564-3.
- [28] I. Stuke, T. Aach, C. Mota, and E. Barth. Estimation of multiple motions: regularization and performance evaluation. 2003 February. ISBN 3-88722-565-1.
- [29] I. Stuke, T. Aach, C. Mota, and E. Barth. Linear and regularized solutions for multiple motions. 2003 February. ISBN 3-88722-566-X.
- [30] W. Horbelt and J. Timmer. Asymptotic scaling laws for precision of parameter estimates in dynamical systems. 2003 February. ISBN 3-88722-567-8.
- [31] R. Dahlhaus and S. Subba Rao. Statistical inference of time-varying arch processes. 2003 April. ISBN 3-88722-572-4.

- [32] G. Winkler, A. Kempe, V. Liebscher, and O. Wittich. Parsimonious segmentation of time series by potts models. 2003 April. ISBN 3-88722-573-2.
- [33] R. Ramlau and G. Teschke. Regularization of sobolev embedding operators and applications. 2003 April. ISBN 3-88722-574-0.
- [34] K. Bredies, D. Lorenz, and P. Maaß. Mathematical concepts of multiscale smoothing. 2003 April. ISBN 3-88722-575-9.
- [35] A. Martin, S.M. Prigarin, and G. Winkler. Exact and fast numerical algorithms for the stochastic wave equation. 2003 May. ISBN 3-88722-576-7.
- [36] D. Maraun, W. Horbelt, H. Rust, J. Timmer, H.P. Happersberger, and F. Drepper. Identification of rate constants and non-observable absorption spectra in nonlinear biochemical reaction dynamics. 2003 May. ISBN 3-88722-577-5.
- [37] Q. Xie, M. Holschneider, and M. Kulesh. Some remarks on linear diffeomorphisms in wavelet space. 2003 July. ISBN 3-88722-582-1.
- [38] M.S. Diallo, M., Holschneider, M. Kulesh, F. Scherbaum, and F. Adler. Characterization of seismic waves polarization attributes using continuous wavelet transforms. 2003 July. ISBN 3-88722-581-3.
- [39] T. Maiwald, M. Winterhalder, A. Aschenbrenner-Scheibe, H.U. Voss, A. Schulze-Bonhage, and J. Timmer. Comparison of three nonlinear seizure prediction methods by means of the seizure prediction characteristic. 2003 September. ISBN 3-88722-594-5.
- [40] M. Kulesh, M. Holschneider, M.S. Diallo, Q. Xie, and F. Scherbaum. Modeling of wave dispersion using continuous wavelet transforms. 2003 October. ISBN 3-88722-595-3.
- [41] A.G. Rossberg, K. Bartholomé, and J. Timmer. Data-driven optimal filtering for phase and frequency of noisy oscillations: Application to vortex flow metering. 2004 January. ISBN 3-88722-600-3.
- [42] Karsten Koch. Interpolating scaling vectors. 2004 February. ISBN 3-88722-601-1.
- [43] O. Hansen, S. Fischer, and R. Ramlau. Regularization of mellin-type inverse problems with an application to oil engineering. 2004 February. ISBN 3-88722-602-X.
- [44] T. Aach, I. Stuke, C. Mota, and E. Barth. Estimation of multiple local orientations in image signals. 2004 February. ISBN 3-88722-607-0.
- [45] C. Mota, T. Aach, I. Stuke, and E. Barth. Estimation of multiple orientations in multi-dimensional signals. 2004 February. ISBN 3-88722-608-9.
- [46] I. Stuke, T. Aach, E. Barth, and C. Mota. Analysing superimposed oriented patterns. 2004 February. ISBN 3-88722-609-7.
- [47] Henning Thielemann. Bounds for smoothness of refinable functions. 2004 February. ISBN 3-88722-610-0.
- [48] Dirk A. Lorenz. Variational denoising in besov spaces and interpolation of hard and soft wavelet shrinkage. 2004 March. ISBN 3-88722-605-4.

- [49] V. Reitmann and H. Kantz. Frequency domain conditions for the existence of almost periodic solutions in evolutionary variational inequalities. 2004 March. ISBN 3-88722-606-2.
- [50] Karsten Koch. Interpolating scaling vectors: Application to signal and image denoising. 2004 May. ISBN 3-88722-614-3.
- [51] Pavel Mrázek, Joachim Weickert, and Andrés Bruhn. On robust estimation and smoothing with spatial and tonal kernels. 2004 June. ISBN 3-88722-615-1.
- [52] Dirk A. Lorenz. Solving variational problems in image processing via projections - a common view on tv denoising and wavelet shrinkage. 2004 June. ISBN 3-88722-616-X.
- [53] A.G. Rossberg, K.Bartholomé, H.U. Voss, and J. Timmer. Phase synchronization from noisy univariate signals. 2004 August. ISBN 3-88722-617-8.
- [54] Markus Fenn and Gabriele Steidl. Robust local approximation of scattered data. 2004 October. ISBN 3-88722-622-4.
- [55] Henning Thielemann. Audio processing using haskell. 2004 October. ISBN 3-88722-623-2.
- [56] M.Holschneider, M. S. Diallo, M. Kulesh, F. Scherbaum, M. Ohrnberger, and E. Lück. Characterization of dispersive surface wave using continuous wavelet transforms. 2004 October. ISBN 3-88722-624-0.
- [57] M. S. Diallo, M. Kulesh, M. Holschneider, and F. Scherbaum. Instantaneous polarization attributes in the time-frequency domain and wave field separation. 2004 October. ISBN 3-88722-625-9.